



Pitting Corrosion of 17-4PH Stainless Steel: Impingement of a Fluid Jet vs. Erosion–Corrosion in the Presence of the Solid Particles

Iman Taji¹ · Mehrdad Hoseinpoor¹ · Mohammad Hadi Moayed¹ · Sohrab Pahlavan¹

Received: 12 July 2020 / Revised: 1 September 2020 / Accepted: 22 September 2020 / Published online: 28 September 2020
© Springer Nature Switzerland AG 2020

Abstract

The pitting corrosion behaviour of 17-4PH (H900) stainless steel during static corrosion (SC), flow-induced corrosion (FIC) and erosion–corrosion (EC) conditions was studied. In comparison with SC, reduction in both corrosion potential (E_{corr}) and pitting potential (E_{pit}) was observed in the EC measurement with sand particles. This behaviour was attributed to the presence of depassivated areas with lower potential on the surface that moves E_{corr} towards lower values and provided favourable locations for pit formation. Acceleration in the access of oxygen to the surface increased meaningfully the E_{corr} in FIC condition and pitting corrosion occurred during open-circuit potential (OCP) measurement in the absence of external polarisation. However, long-term OCP measurements in SC and EC circumstances did not show stable pitting. Consequently, it was proposed that in some conditions, the FIC without eroding particles could be more detrimental compared to slurry EC.

Keywords Stainless steel · Pitting · Solid particle erosion · Fluid induced corrosion

1 Introduction

Erosion is a common phenomenon when the working environment is associated with solid and/or liquid impacts on the surface [1]. Such circumstances are observed in various engineering applications like pumps, agitators, valves, pipelines and drilling conditions [2–4]. As the liquid is also present in some cases, it is possible to observe corrosion accompanied by the mentioned erosion. Hence, the so-called erosion–corrosion (EC) process has been a problem investigated for many suchlike systems [3, 5–10].

Published literature about EC predominantly focused on a synergism appears between erosion and corrosion. This synergism means that the existence of erosion together with corrosion causes the total wear rate to be greater than the simple summation of the rates when the two processes act independently [11–14]. The synergism seems to be more severe when the erodent impacts the surface at more oblique angles due to more surface denudation [11]. It is believed that accelerated oxygen mass transfer [8, 15, 16], passive

film breakdown by solid impacts [17], surface roughening by erosion [15, 17, 18] and the enhanced crack growth by corrosion [7] can be the most important phenomena in EC mechanisms. It has also been reported that stainless steel (SS) susceptibility to pitting corrosion increases in the presence of an erosive environment [17].

The pitting corrosion is a kind of localised corrosion which may degrade the alloys capable of forming a passive film on their surface, in the presence of some species known as aggressive ions. When the passivity is lost, the underlying alloy dissolution would be accelerated [19–21]. The pitting corrosion does not extend over the alloy surface; instead it propagates into the interior and can cause majority of failures in metallic structures [22]. This is why it is of great concern for passive alloys, and especially for the SSs [20, 23–28].

Martensitic precipitation-hardening (PH) SSs are a useful alloy family for demanding applications requiring high mechanical properties and corrosion resistance [29]. Investigating the effect of ageing temperature on EC behaviour of 17-4PH SS revealed that the least EC rate is obtained at the ageing temperature when the highest hardness is reached [2]. Likewise, the proper low-temperature nitriding is perceived to improve the EC resistance of 17-4PH SS [30]. However, there is a lack of data in relevant literatures on the comparison between flow-induced corrosion (FIC) damage without

✉ Mehrdad Hoseinpoor
ziahosem@vscht.cz

¹ Metallurgical and Material Engineering Department,
Faculty of Engineering, Ferdowsi University of Mashhad,
91775-1111 Mashhad, Iran

any solid particles and slurry EC with solid particles for this alloy. Clarifying the dominant EC mechanisms, eventually, would help us to control the expenses either by EC inhibition or by material substitution.

In this work, the pitting corrosion behaviour of the heat-treated 17-4PH SS specimens is examined by means of polarisation techniques in static corrosion (SC), FIC and EC conditions. A comparison between these three conditions is made to clarify the influence of them on the pitting corrosion behaviour of the metal. By comparing EC and FIC conditions, it is proposed that FIC can have more detrimental corrosion damage rather than EC with solid particles.

2 Experimental Procedures

2.1 Materials and Preparations

The chemical composition of 17-4PH SS used in this study has been listed in Table 1. Specimens were first solution annealed at 1040 °C for 1 h. Afterwards, samples were heat treated to H 900 specification. The samples were cut into cubes approximately 10×10×10 mm³ in size and mounted in an inert epoxy resin polymer.

The test solution used for the SC and FIC conditions was 3.5 wt% NaCl solution made by distilled water and salt chemical reagent. The EC experiments were carried out in a solution consisting of 3.5 wt% NaCl + 3 wt% silica sand

particles. Sand sizes were varied in the range 210–297 μm, separated with standard sieves. Assessment of the applied sand showed that the particles mostly had the roundish shape without significant edges.

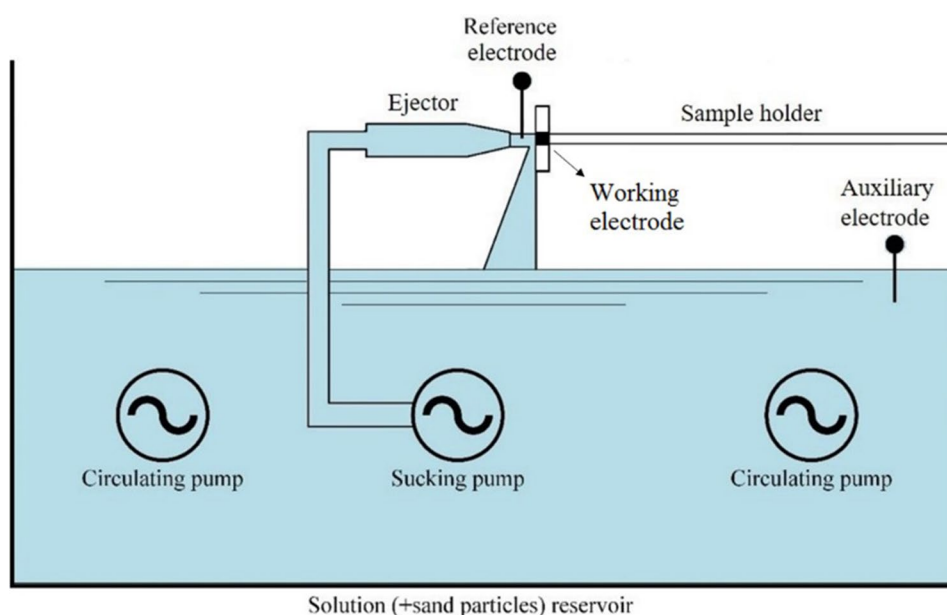
2.2 Apparatus for Flow-Induced Corrosion and Erosion–Corrosion Tests

All EC tests were performed by an apparatus of impinging jet which has been illustrated in Fig. 1, schematically. The apparatus was designed based on Zu, Hutchings and Burstein's work [31] with some differences in feeding the sand particles. The reservoir commonly contained 15 L of the test solution and was open to the air. Two pumps were used to circulate the test solution in order to attain homogeneity and prevent the sand precipitation. Another discrete sucking pump was utilised to drive the solution up to the PVC nozzle (5 mm) by means of a hose. All parts of the pumps were made of non-metallic equipment. The impinging jet direction was perpendicular to the specimen surface. The distance between the nozzle exit and the working electrode was 10 mm. The impact velocity was calculated by dividing the discharge rate of water by the cross-sectional area of the nozzle. In this way, the mean impact velocity was calculated as 3 m/s. The concentration of the particles in the slurry was determined by weighing a given volume of collected slurry for a constant period of time (ca. 3 wt%).

Table 1 The chemical composition (in wt%) of 17-4PH SS studied in this work

Fe	Cr	Ni	Cu	Mn	Nb	Si	Mo	C	P	V	S
Bal.	15.09	4.59	4.14	0.61	0.358	0.32	0.18	0.04	0.018	0.013	0.012

Fig. 1 The schematic diagram of EC apparatus used in this work. Two circulating pumps were homogenised the slurry and the medial one pumped the slurry up towards the working electrode surface. Reference electrode was situated frontward the ejector in contact with the slurry and auxiliary electrode was placed somewhere in reservoir



2.3 Electrochemical Experiments

To investigate the electrochemical behaviour of 17-4PH (H900) SS under the EC condition, the classic three-electrode designation with the saturated calomel reference electrode (SCE) and platinum counter electrode was used. The situations of the electrodes have been shown in Fig. 1.

Potentiodynamic polarisation carried out with the scanning rate of 60 mV/min, started from -50 mV below open-circuit potential (OCP). The scan direction reversed while the current indicated that stable pitting or transpassivity had occurred. Potentiostatic polarisation, at the constant potential of -150 mV (SCE) and data acquisition rate of 1 Hz, was also performed in order to examine the passivity state of the alloy. Before the measurements, open-circuit potential was measured for 30 min in both methods. The electrochemical measurements were performed by the Gill AC (ACM instruments) potentiostat.

2.4 SEM Images

Scanning electron microscopy (SEM) images of the eroded samples were recorded using LEO VP 1450. Prior to the experiment, the samples were wet grinded with SiC paper and mirror-polished using a polishing cloth down to the $1\ \mu\text{m}$ diamond paste. The similar preparation procedure was applied after the experiment for crosscut evaluation.

3 Results

3.1 Open-Circuit Behaviour

The OCP in the three studied conditions is depicted in Fig. 2. Recording started right after the sample was exposed to the test solution.

Three distinct regions that are believed to exist in the FIC state [8] are observed here as well. First, the region with increasing potential trend which has been established by accelerated passive film formation. Following this ascendant trend, the significant potential drop is occurred at the border between regions one and two. This potential drop can be attributed to the formation of stable pit on the surface after induction time (T_{ind}). Furthermore, in the second region, there are some fluctuations initiated by metastable pits nucleation, growth, and repassivation. At third region, by further stabilisation of the pit, the E_{corr} decreases smoothly and reaches to a value of about -270 mV (SCE).

Regarding to SC, the OCP starts from -250 mV (SCE) and gradually reaches to about -140 mV (SCE). However, the OCP for the EC begins at much lower value of about -420 mV (SCE) and slowly goes up to about -300 mV (SCE). There are also a lot of fluctuations representing the

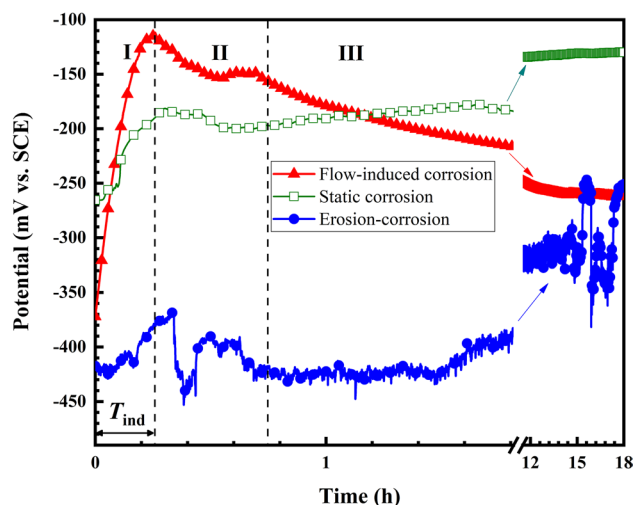


Fig. 2 Open-circuit potential measurements under the SC, FIC and EC conditions

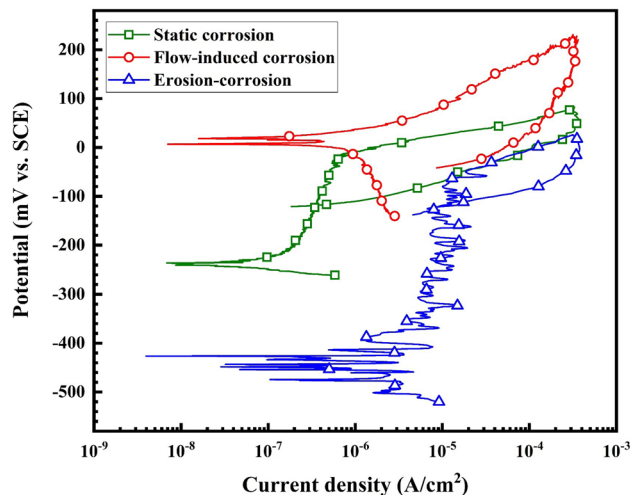


Fig. 3 Potentiodynamic curves obtained in the SC, FIC and EC conditions.

depassivation events caused by the solid particle impacts. In contrast to FIC, the general trend of potential for SC and EC conditions is increasing.

3.2 Potentiodynamic Behaviour

Figure 3 illustrates the potentiodynamic curves obtained in different conditions. As it can be observed, in 3.5 wt% NaCl solution, 17-4PH (H900) SS remains passive in the SC and EC conditions, while in the case of the FIC, there is no evident passivity and sample indicates active state. This behaviour ascertains the presence of stable pit on the surface. Clearly, there are more transients standing on anodic

Table 2 Comparison of E_{corr} and E_{pit} 17-4PH (H900) SS samples in the SC, FIC and EC conditions

E_{corr} (mV/SCE)			E_{pit} (mV/SCE)		
SC	EC	FIC	SC	EC	FIC
-260 ± 10	-450 ± 10	-20 ± 15	0 ± 10	-50 ± 5	NA

NA not available

branch of the EC curves compared to the other two. As mentioned, these transients are representing the depassivation events caused by the impact of the sand particles. In addition, the cathodic branch related to FIC condition is larger compared to other condition. This behaviour may arise from the unstable condition formed by pitting corrosion.

According to Fig. 3, it is clear that three distinct parameters must be taken into consideration in these different conditions including the pitting potential (E_{pit}), the corrosion potential (E_{corr}), and the passivity range.

Table 2 presents the average values E_{corr} and E_{pit} for different conditions. The lowest and highest values of E_{corr} belong to the EC and FIC conditions, respectively. Erosion strongly reduces the corrosion potential down to about -450 mV (SCE), while E_{corr} under the impinging circumstance has a noticeable high value and stands near to the range of potentials at which the specimens in the SC and EC conditions will be pitted. Furthermore, the E_{pit} value related to EC condition is almost 50 mV lower compared to SC ones. It should be noted that according to Fig. 3, the E_{pit} was not assignable under the FIC condition and the alloy did not show any state of passivity.

3.3 Potentiostatic Polarisation

Figure 4 compares the passivity behaviour at the potential of -150 mV (SCE) for the SC and EC conditions. At this specific potential, 17-4PH (H900) SS would be passive in 3.5 wt% NaCl solution under the two mentioned conditions, while in the case of the FIC, there is no state of passivity for this alloy, see Fig. 3.

As shown, the i_{pass} in the EC state is significantly higher compared to SC and there are abundant transients in current. The substantial difference in the size and density of the existing fluctuations under the SC and EC conditions can be noticed better by considering the magnified section. The current transients on the EC curve are nearly 100 times larger than SC ones. As abovementioned, the depassivation events caused by collision of the solid particle to the surface can originate these abundant transients. However, the fluctuation of the current density in SC condition originates from metastable pitting [32, 33]. During measurement, the background current density is reduced by healing of the passive layer on the surface [34].

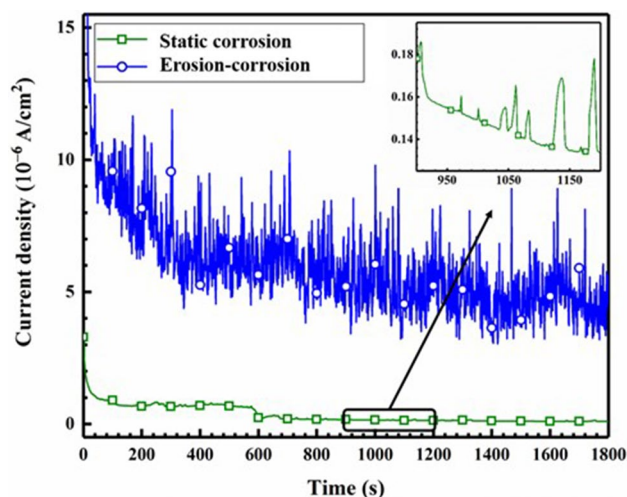


Fig. 4 Typical potentiostatic experiments under SC and EC conditions

4 Discussion

4.1 Slurry Erosion–Corrosion

The results represented in Figs. 3 and 4 confirm that the i_{pass} is increased and the E_{pit} is reduced by EC. These results are in line with previous reports that the erosion caused by solid impacts can lead to the increase of the current recorded by the potentiostat as a result of the surface denudation and also to the reduction of E_{pit} [17]. The higher passive current density can be attributed to the continuous deterioration of the passive layer caused by solid particles. Furthermore, SEM micrographs after EC measurement show a surface with high roughness in contact to the corrosive environment, see Fig. 5. Evident plastic deformation traces in these micrographs divulge the numerous local depassivations caused by solid particle impacts. They confirm that in the presence of the solid particles, the passive surface is repeatedly deteriorated. Besides, it is evident that how the surface is roughened by the impact of the solid particles. It is well known that both the pit nucleation and growth processes are promoted by increasing the surface roughness [15, 18]. Thus, E_{pit} is reduced by the solid particle impacts on the surface, compared to when the condition is static.

However, the lower E_{corr} for the EC condition has another reason. Generally, by testing in hydrodynamic condition (FIC and EC), the E_{corr} increases as the oxygen feeding on the metal surface is facilitated in comparison with the static condition and accelerates the cathodic reaction, see Fig. 6. Though, considering the depassivation-induced transients observed in the abovementioned figures, it can be said that the surface under the erosive circumstance, would be partitioned into two parts: active or depassivated areas and passive regions. By impact of each particle to the surface,

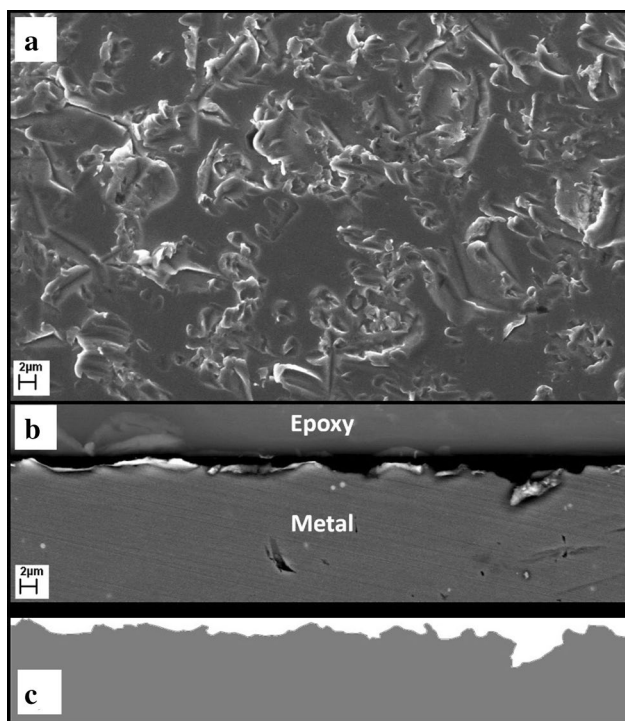


Fig. 5 Scanning electron micrographs for a 17-4PH SS (H900) specimen exposed to an EC experiment: **a** top view (EHT: 20 kV, Observation mode: SE); **b** side view (EHT: 20 kV, Observation mode: BSD); **c** schematic diagram of the solid impacts on the metal surface

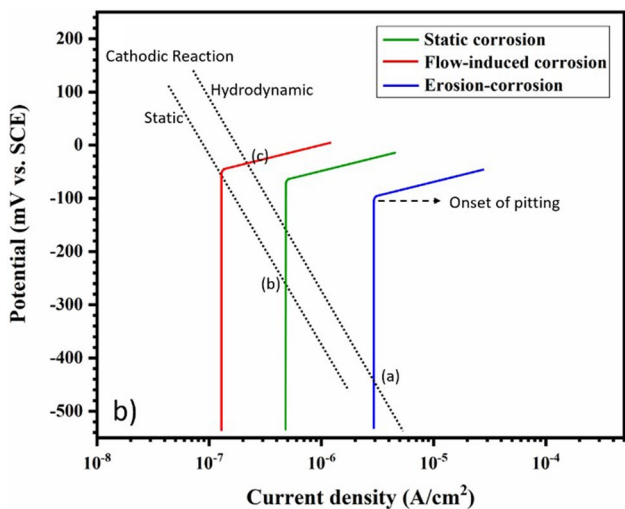


Fig. 6 The variation of E_{corr} and anodic/cathodic branches for SC, FIC and EC conditions

the passive layer can be damaged and separated from the metallic sub-surface. Therefore, at the resultant depassivated parts, the bare surfaces are directly exposed to the solution. The passive and active regions are continuously formed on the metal surface during the EC test and due to

the significant lower potential of the active areas compared to passive parts, the E_{corr} moves toward lower values. The decrement would be hence dependent on the solid particles' concentration and the impact velocity. This is consistent with what was found in the work of Wharton et al. [35] on the effect of the flow velocity on the EC of 316L SS. Their results showed that when the velocity exceeded a critical value, the E_{corr} decreased until it reached to about -420 mV (SCE), which is comparable to the current work's measurements.

4.2 Flow-Induced Corrosion

It was reported that in the absence of solid particles, under the fluid jet impinging circumstance, the E_{pit} is increased, and the stable pitting could be retarded [8, 16]. However, based on the presented results, 17-4PH (H900) SS specimen is unlikely pitted in the case of FIC. It is believed that pitting corrosion in FIC is hindered mainly in smaller specimen areas [8]. Regarding to the performed measurements, the drastic rise in the corrosion potential under the impinging condition accelerates pitting. According to Fig. 6, this increment in E_{corr} is due to both the cathodic reaction acceleration and the anodic reaction inhibition. As known, in the FIC condition, acceleration of oxygen feeding to the surface enhances the formation of the passive layer and reduces the passive current density. Therefore, according to Fig. 6, the anodic and cathodic reactions intersect at potential higher than the E_{pit} (point c). As a result, no passivity can be observed in the potentiodynamic polarisation of the FIC curves. In fact, when the anodic scan is started in the FIC condition, stable pits have already formed on the sample surface. As is also evident in Fig. 2, the corrosion potential of the sample in the FIC condition lays approximately in the range of the pitting potentials obtained for other conditions.

4.3 Flow-Induced Corrosion vs. Erosion-Corrosion

According to what was explained above, there is a kind of hesitance in comparing the fluid jet FIC and slurry EC. On one side, the EC in the presence of sand particles possesses higher passive current density which leads to a higher amount of corrosion in comparison with the FIC. However, on the other side, the FIC circumstance is very unfavourable due to the fast formation of stable pit under the open-circuit control condition. Consequently, in long-term exposure, the localised corrosion which is occurred in the FIC condition could be more detrimental than the one observed by EC damages. It should be noted that the occurrence of pitting and the value of the i_{pass} are highly dependent on the test or exposure conditions. The impingement speed and angle, the chemical composition of the solution, and the shape, size and density of the solid particles are the main parameters

that could change the corrosion mode of metal. However, it seems that in our experimental condition, the FIC has been more detrimental due to the stabilisation of the localised corrosion in the OCP condition.

5 Conclusions

1. FIC increases the E_{corr} of 17-4PH (H900) SS as a result of the cathodic reaction acceleration and enhancement of passive layer formation. Accordingly, at open-circuit control, stable pitting occurs after about 15 min. No stable pitting is observed during long-term OCP measurement in the EC and SC conditions.
2. The EC lowers E_{corr} largely due to the depassivation events made by solid impacts. This depassivation exposes some bare steel surfaces with low potential to the solution and subsequently decreases the whole surface potential.
3. The passive film ruptures caused by erosion increase the occurrence of metastable pits. There are observable transients on the OCP background of the EC case, accordingly.
4. The results reveal that by EC measurement, the surface roughness is increased and the nucleation and pitting growth process are promoted and the E_{pit} is reduced.
5. The immediate development of stable pitting in the FIC condition makes it more detrimental than the other circumstances.

Acknowledgements Authors would like to appreciate the financial support from Ferdowsi University of Mashhad provision of laboratory facilities during the period that this research was conducted.

References

1. Bargmann HW (1992) The mechanics of erosion by liquid and solid impact. *Intl J Solids Struct* 29(14–15):1685–1698
2. Ping L, Cai Q-z, Wei B-k, Zhang X-z (2006) Effect of aging temperature on erosion–corrosion behavior of 17-4PH stainless steels in dilute sulphuric acid slurry. *J Iron Steel Res Intl* 13(5):73–78
3. Postlethwaite J, Tinker E, Hawrylak M (1974) Erosion–corrosion in slurry pipelines. *Corrosion* 30(8):285–290
4. Reyes M, Neville A (2001) Mechanisms of erosion–corrosion on a cobalt-base alloy and stainless-steel UNS S17400 in aggressive slurries. *J Mater Eng Perform* 10(6):723–730
5. Abedini M, Ghasemi H (2014) Synergistic erosion–corrosion behavior of Al–brass alloy at various impingement angles. *Wear* 319(1–2):49–55
6. Barik R, Wharton J, Wood R, Tan K, Stokes K (2005) Erosion and erosion–corrosion performance of cast and thermally sprayed nickel–aluminium bronze. *Wear* 259(1–6):230–242
7. Li Y, Burstein G, Hutchings I (1995) The influence of corrosion on the erosion of aluminium by aqueous silica slurries. *Wear* 186:515–522
8. Sasaki K, Burstein G (2007) Erosion–corrosion of stainless steel under impingement by a fluid jet. *Corros Sci* 49(1):92–102
9. Zeng L, Zhang G, Guo X (2014) Erosion–corrosion at different locations of X65 carbon steel elbow. *Corros Sci* 85:318–330
10. Zhao Y, Zhou F, Yao J, Dong S, Li N (2015) Erosion–corrosion behavior and corrosion resistance of AISI 316 stainless steel in flow jet impingement. *Wear* 328:464–474
11. Burstein G, Sasaki K (2000) Effect of impact angle on the slurry erosion–corrosion of 304L stainless steel. *Wear* 240(1–2):80–94
12. Burstein G, Sasaki K (2001) Detecting electrochemical transients generated by erosion–corrosion. *Electrochim Acta* 46(24–25):3675–3683
13. Wood RJ (2006) Erosion–corrosion interactions and their effect on marine and offshore materials. *Wear* 261(9):1012–1023
14. Zhou S, Stack M, Newman R (1996) Characterization of synergistic effects between erosion and corrosion in an aqueous environment using electrochemical techniques. *Corrosion* 52(12):934–946
15. Postlethwaite J, Dobbin M, Bergevin K (1986) The role of oxygen mass transfer in the erosion–corrosion of slurry pipelines. *Corrosion* 42(9):514–521
16. Zheng Z, Zheng Y (2016) Erosion-enhanced corrosion of stainless steel and carbon steel measured electrochemically under liquid and slurry impingement. *Corros Sci* 102:259–268
17. Burstein G, Sasaki K (2000) The birth of corrosion pits as stimulated by slurry erosion. *Corros Sci* 42(5):841–860
18. Sasaki K, Burstein G (1996) The generation of surface roughness during slurry erosion–corrosion and its effect on the pitting potential. *Corros Sci* 38(12):2111–2120
19. Farjami A, Yousefnia H, Seyedraoufi Z-S, Shajari Y (2020) Investigation of inhibitive effects of 2-mercaptobenzimidazole (2-MBI) and polyethyleneimine (PEI) on pitting corrosion of austenitic stainless steel. *J Bio- Tribo-Corros* 6(3):1–19
20. Loto RT, Loto CA (2019) Comparative assessment of the pitting corrosion resistance and passivation behaviour of 439L ferritic and 904L austenitic stainless steels for application in extreme process environments. *J Bio- Tribo-Corros* 5(3):57
21. Taji I, Moayed MH, Mirjalili M (2015) Correlation between sensitisation and pitting corrosion of AISI 403 martensitic stainless steel. *Corros Sci* 92:301–308
22. Tan H (2003) Combined atomistic and continuum simulation of fracture and corrosion
23. Frankel GS, Li T, Scully JR (2017) Perspective—localized corrosion: passive film breakdown vs pit growth stability. *J Electrochem Soc* 164(4):C180
24. Hoseinpoor M, Momeni M, Moayed MH, Davoodi A (2014) EIS assessment of critical pitting temperature of 2205 duplex stainless steel in acidified ferric chloride solution. *Corros Sci* 80:197–204
25. Li T, Scully J, Frankel G (2018) Localized corrosion: passive film breakdown vs. pit growth stability: part III. A unifying set of principal parameters and criteria for pit stabilization and salt film formation. *J Electrochem Soc* 165(11):C762
26. Pahlavan S, Moayed MH, Mirjalili M (2019) The contrast between the pitting corrosion of 316 SS in NaCl and NaBr solutions: part II. Morphology, chemistry, and stabilization of the pits. *J Electrochem Soc* 166(12):C321
27. Pahlavan S, Moayed MH, Mirjalili M (2019) The contrast between the pitting corrosion of 316 SS in NaCl and NaBr solutions: part I. Evolution of metastable pitting and stable pitting. *J Electrochem Soc* 166(2):C65
28. Pal S, Bhadauria SS, Kumar P (2019) Pitting corrosion behavior of F304 stainless steel under the exposure of ferric chloride solution. *J Bio- Tribo-Corros* 5(4):91
29. McGuire MF (2008) *Stainless steels for design engineers*. ASM International, Cleveland

30. Wang J, Lin Y, Li M, Fan H, Zeng D, Xiong J (2013) Effects of the treating time on microstructure and erosion corrosion behavior of salt-bath-nitrided 17-4PH stainless steel. *Metall Mater Trans B* 44(4):1010–1016
31. Zu J, Hutchings I, Burstein G (1990) Design of a slurry erosion test rig. *Wear* 140(2):331–344
32. Moayed M, Newman R (2006) Evolution of current transients and morphology of metastable and stable pitting on stainless steel near the critical pitting temperature. *Corros Sci* 48(4):1004–1018
33. Pistorius P, Burstein G (1992) Metastable pitting corrosion of stainless steel and the transition to stability. *Philos Trans R Soc Lond Series A* 341(1662):531–559
34. Pyun S-I, Hong M-H (1992) A model describing the growth kinetics of passivating oxide film prepared under potentiostatic conditions. *Electrochim Acta* 37(2):327–332
35. Wharton J, Wood R (2004) Influence of flow conditions on the corrosion of AISI 304L stainless steel. *Wear* 256(5):525–536

Publisher's Note Springer Nature remains neutral with regard to jurisdictional claims in published maps and institutional affiliations.